Wind and Structures, *Vol. 28, No. 1 (2019) 1-17*
DOI: https://doi.org/10.12989/was.2019.28.1.001

The influence of internal ring beams on the internal pressure for large cooling towers with wind-thermal coupling effect

Shitang Ke[*1,2], Wei Yu[1a], Yaojun Ge[2b], Lin Zhao[2c] and Shuyang Cao[2d]

[1]*Department of Civil Engineering, Nanjing University of Aeronautics and Astronautics, 29 Yudao Street, Qinhuai District, Nanjing, Jangsu Province, China*
[2]*State Key Laboratory for Disaster Reduction in Civil Engineering, Tongji University, 1239 Sping Road, Yangpu District, Shanghai, China*

(Received September 8, 2018, Revised November 3, 2018, Accepted November 7, 2018)

Abstract. Internal ring beams are primary components of new ring-stiffened cooling towers. In this study, numerical simulation of the internal flow field of a cooling tower with three ring beams under wind-thermal coupling effect is performed. The studied cooling tower is a 220-m super-large hyperbolic indirect natural draft cooling tower that is under construction in China and will be the World's highest cooling tower, the influence of peripheral radiators in operating cooling tower is also considered. Based on the simulation, the three-dimensional effect and distribution pattern of the wind loads on inner surface of the cooling tower is summarized, the average wind pressure distributions on the inner surface before and after the addition of the ring beams are analyzed, and the influence pattern of ring beams on the internal pressure coefficient value is derived. The action mechanisms behind the air flows inside the tower are compared. In addition, the effects of internal ring beams on temperature field characteristics, turbulence kinetic energy distribution, and wind resistance are analyzed. Finally, the internal pressure coefficients are suggested for ring-stiffened cooling towers under wind-thermal coupling effect. The study shows that the influence of internal stiffening ring beams on the internal pressure and flow of cooling towers should not be ignored, and the wind-thermal coupling effect should also be considered in the numerical simulation of cooling tower flow fields. The primary conclusions presented in this paper offer references for determining the internal suction of such ring-stiffened cooling towers.

Keywords: indirect natural draft cooling tower; numerical simulation; wind-thermal coupling; internal ring beam; internal pressure effect

1. Introduction

Cooling towers are high-rise thin-shell structures that are subjected to wind loads (Li *et al.* 2017). As the size of cooling towers is getting bigger and bigger, the safety and stability of large-scale cooling towers under strong wind loads are drawing much attention (Zhao *et al*. 2014, Ke *et al.* 2018). In practical application, suitable approaches (Babu *et al.* 2013, Burger 2014) are applied to solve the wind-resistance and stability issues brought by the scaling-up of cooling towers. Existing studies (Sabouri-Ghomi *et al.* 2006, Zhang *et al*. 2014) have shown that internal stiffening ring beams effectively increase towering structures' overall stiffness and stability under static wind loads.

In the current guidelines for cooling tower design (VGB-R 610Ue 2005; GB/T 50102-2014 2014), the effect of internal suction is included in the calculation of stability, and the empirical values of internal pressure coefficient are also given. The effect of internal pressure makes a cooling tower structure subject to circumferential pressure and reduces its stability, thus it has to be considered for the wind resistance design of cooling towers. Many scholars have carried out studies to investigate the wind loads on the inner surfaces of cooling towers. Sollenberger and Billington performed field measurement of wind pressure in cooling towers and reckoned that the internal pressure is constant and the wind pressure coefficient is -0.4 on the inner surface of cooling towers (Sollenberger and Billington 1980). Sun and Zhou made a field measurement of the internal wind pressure distribution of Maoming cooling tower. The results show that the inner pressure is evenly distributed along the zonal under low wind speed, while the inner pressure is uneven the strong wind (Sun and Zhou 1983). Kawarabata et al. proposes that the internal pressure coefficient is in a value range of -0.5 to -0.4, and suggests to use -0.4 for practical design of cooling towers (Kawarabata *et al.* 1983). Based on wind tunnel experiments, Kasperski and Niemann concluded that inside a cooling tower, the pressure is evenly distributed both circumferentially and vertically, and the pressure coefficient is around -0.5 (Kasperski and Niemann 1988). Zhao and Ge performed measurements of internal wind pressure distribution of taps under the various ventilation ratios ranging from 0% to 100% (Zhao and Ge 2010). By using realizable k-ε turbulence model and multi-phase flow model,

*Corresponding author, Professor
E-mail: keshitang@163.com
[a] Postgraduate
E-mail: yuweinuaa@163.com
[b] Professor
E-mail: yaojunge@tongji.edu.cn
[c] Professor
E-mail: zhaolin@tongji.edu.cn
[d] Professor
E-mail: shuyang@tongji.edu.cn

http://www.techno-press.com/journals/was&subpage=7 ISSN: 1226-6116 (Print), 1598-6225 (Online)

Shen et al. simulated the hot-cold air self-circulation system formed from natural wind sources as well as the internal surface wind load under external wind field effect; the calculation shows that the internal pressure generated from external wind field effect varies significantly with elevation and latitude, and the average values of internal pressure coefficients is in a range of -0.43 to -0.52 (Shen *et al*. 2011). In addition, the internal pressure of the cooling tower whether considering herringbone column or not is discussed. The results showed that the internal pressure is -0.4 when the herringbone column is considered and the internal pressure reduce 0.3 when the herringbone column is not considered (Shen *et al*. 2011). Goudarzi and Sabbagh-Yazdi made comparison between internal and external pressure distributions performed a full scale cooling tower and the VGB suggestion (Goudarzi and Sabbagh-Yazdi 2011), the internal negative pressure reduce at most of internal parts of the cooling tower. Ke *et al*. performed hydro-mechanical numerical simulation to generalize the impact pattern of the louvers' air flow rate of large-scale indirect air cooling towers; the study shows that as the air flow rate increases, the internal pressure coefficient decreases (Ke *et al*. 2015). Based on rigid pressure test, Zou *et al*. analyzed the three-dimensional effects of the cross baffles on the surface wind pressure inside cooling towers; the study shows that the inner surface pressure is not evenly distributed along vertical or circumferential direction, the value of internal pressure can be -0.5 (Zou *et al.* 2015, Zou *et al.* 2015). Dong et al. obtained the internal wind pressure of natural draft counter-flow wet cooling tower under operating conditions, the average of the total internal pressure coefficient of the tower under type-B landforms is -0.449 (Dong *et al.* 2015). Dong et al. simulated the effect of the internal components of super-large cooling towers, such as cross baffles and packing, on the average internal surface wind load; the simulation result shows that the rectification effect of internal components reduces the absolute value of internal pressure (Dong *et al.* 2016).

Existing studies have not reached an agreement on the wind load distribution on inner surface of cooling towers. Regarding external factors that influence the internal flow field distribution of cooling towers, cross baffles, packing, and other internal components are the primary influencing factors for natural draft counter-flow wet cooling towers. However, for indirect cooling towers, natural draft dry cooling (Du *et al.* 2014, Gu *et al.* 2016) is commonly employed; the towers are open and clear inside with concentrated louver radiators surrounding them. Existing studies have investigated the influences of air flow rate and extension platforms on the pressure on inner surface of cooling towers (Zhao *et al.* 2010, Ke *et al*. 2015). Although ring-stiffened cooling towers have great potential in the future, the influence of ring beams on the internal pressure of indirect air cooling towers with peripheral radiators' heating effect considered has rarely been studied.

In this study, a super-large hyperbolic indirect natural draft cooling tower 220 m high that is under construction in China is investigated, and it will be the World's highest cooling tower. Based on computational fluid dynamics (Sarjito 2014, Wittek and Grote 2015), the internal surface wind loads of the tower are study, which has three horizontal stiffening rings designed installed, with the wind-thermal coupling effect considered. The three-dimensional effect and distribution pattern of the wind load on inner surface of the cooling tower is summarized, the average wind pressure distributions on the inner surface before and after the addition of the ring beams are analyzed, and the influence pattern of ring beams on the internal pressure is derived. The mechanisms behind the air flows inside the tower are compared. In addition, the effects of internal ring beams on temperature field characteristics, turbulence kinetic energy distribution, and wind resistance are analyzed. Finally, the internal pressure coefficients are suggested for ring-stiffened cooling towers under wind-thermal coupling effect.

2. Project overview

The studied super-large hyperbolic indirect natural draft cooling tower has a total height of 220 m, a throat elevation of 165 m, an air inlet elevation of 30.75 m, a tower top plane diameter of 128.1 m, a throat plane diameter of 123 m, and a tower bottom diameter of 185 m. Fig. 1 shows wall thickness and radius of cooling tower along the height. The minimum wall thickness of cooling tower is 0.38 m, and the maximum thickness is 1.85 m. The tower tube is supported and connected to the hoop base by 64 pairs of X-shaped props. The cross sections of the X-shaped props are rectangle with the size of 1.7 m×1.0 m. The hoop base is a cast-in-place reinforced concrete structure that is 10.5 m in width and 2.2 m in height. To study the effects of internal stiffening ring beams on internal pressure, two designs for the studied cooling tower are investigate, one regular design and another with stiffening ring beams added. For the latter, three horizontal ring beams are set below the tower throat at the heights of 72.75 m, 94.80 m, and 139.43 m, respectively. Along the vertical direction, the ring beams' average thickness is 0.4 m, and along the radial direction, the beams are in the sizes of 0.71 m, 0.72 m, and 0.74 m, respectively. Fig. 2 illustrates the three-dimensional models of the two designs for the studied cooling tower.

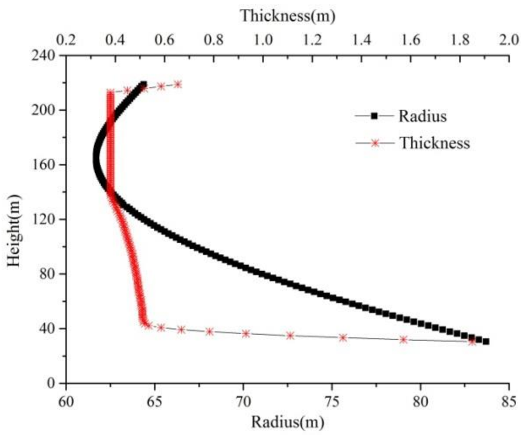

Fig. 1 Wall thickness and radius of cooling tower along the height

Table 1 Calculating conditions of internal pressure

Calculating condition	Cooling tower type	Environmental condition
1	Regular	External wind field
2	Regular	External wind field + temperature field
3	Ring-stiffened	External wind field
4	Ring-stiffened	External wind field + temperature field

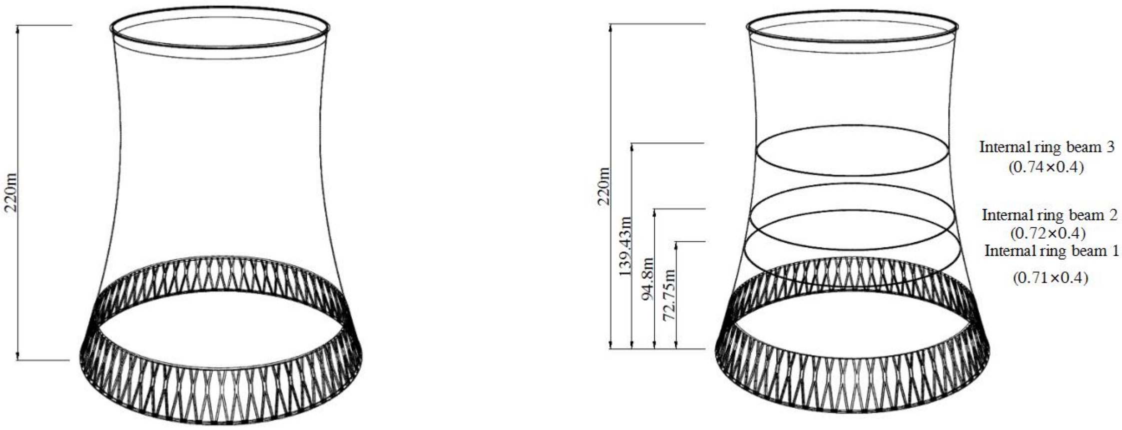

(a) Regular cooling tower (b) Ring-stiffened cooling tower

Fig. 2 Three-dimensional models of the regular cooling tower and the ring-stiffened cooling tower

Indirect air cooling towers are operated by mixed condensers. Inside the thin-shell structure of a cooling tower is a complex system with multiple components. In an operating cooling tower, heat exchange happens between the air cooling radiators and the recirculating water. Therefore, the influence of temperature field on the internal pressure should be considered.

Based on the principle of radiating area equivalency, the complicated radiators around the cooling system are treated as equivalent cuboid units with thermal sources. To investigate the influences of internal ring beams and wind-thermal coupling on the internal pressure of cooling towers, four calculating conditions are designed as shown in Table 1.

3. Numerical simulation

3.1 Mesh generation of the computational domain

The calculation model simulates a tower in the height (H) of 220 m and the bottom diameter (D) of 185 m. A 30% air flow rate is considered for the radiator louvers' open effect during operation (Ke et al. 2015). The computational domain is in the size of X = 20 D along-wind, Y = 16 D across-wind, and Z = 4 H vertically. The cooling tower was setup in the center of the calculating domain to ensure that the wake flow can fully develop. The domain's blocking rate is 1.2% which satisfies the requirement of lower than 5% (JGJ/T 338-2014 2014). With overall consideration of both precision and efficiency, the entire computational domain is partitioned into a regular peripheral area and a complicated core area. Tetrahedral mesh is used for the core area, so as to accurately capture the flow and heat transfer characteristics of fluid in the area and to encrypt the local mesh around the cooling tower. Hexahedral mesh is used for the regular peripheral area, and the number of meshes reaches 12 million. Fig. 3 shows the meshing of the computational domain.

3.2 Calculation parameter configuration

Fig. 4 shows the boundary conditions for the computational domain. Velocity inlet boundary conditions are defined. According to the wind speed in type-B landforms in China and the distribution form of turbulence intensity (as stated in GB50009-2012 2012), the boundary conditions are defined as below.

$$U_z = U_0 (Z / Z_0)^{\alpha} \tag{1}$$

$$I_z(z) = I_{10}(z/10)^{-\alpha} \tag{2}$$

In Eqs. (1) and (2), the value of U_0 is 28.3 m/s; it is the 10-minute maximum average wind speed at the height of Z_0 = 10 m in a 50-year reoccurrence period in the region that the cooling tower is located in; Z is distance of the calculation height to the ground, I_{10} is the nominal turbulence intensity at the height of 10 m and its value is 0.14, and the ground roughness coefficient α is given a value of 0.15.

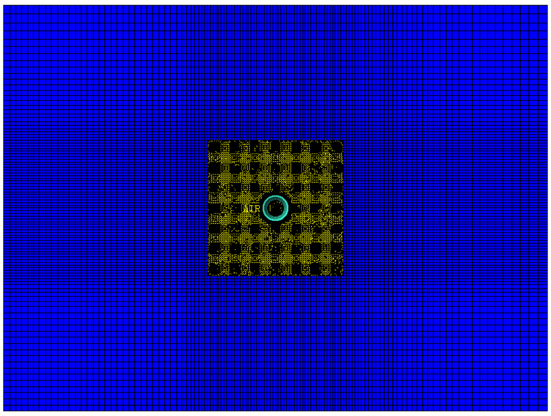

(a) Meshing of the x-y cross section

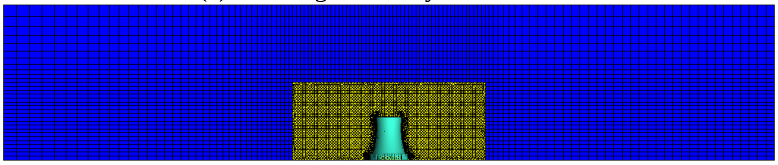

(b) Meshing of the x-z cross section

Fig. 3 Mesh generation of the computational domain for the cooling tower's numerical simulation

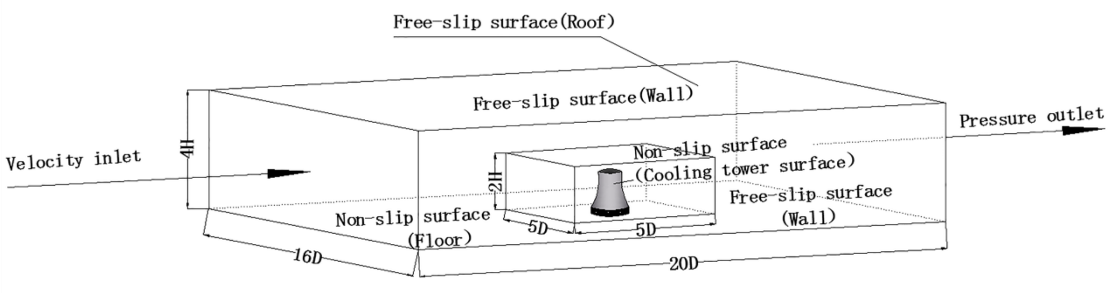

Fig. 4 Boundary conditions of the computational domain

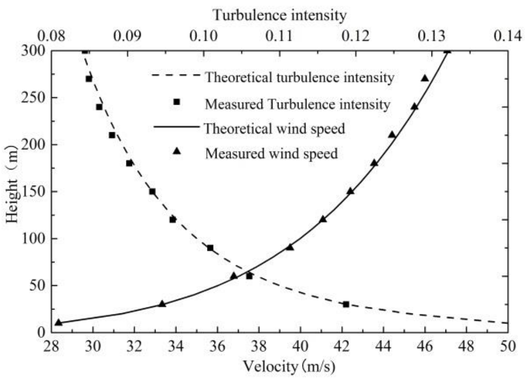

(a) Velocity and turbulence intensity

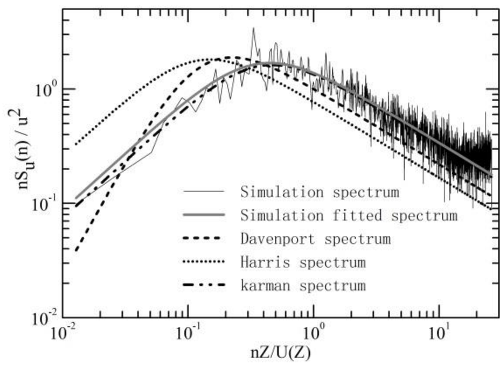

(b) Fluctuation wind speed spectrum

Fig. 5 Velocity and turbulence profiles

By using user-defined functions of the FLUENT software, the above boundary condition is implemented (as seen in Fig. 5). Pressure outlet boundary conditions are defined, and the relative pressure is defined as 0. The ground surface and cooling tower surface of the computational domain are non-slip surfaces, and symmetric boundary conditions are adopted for the walls and roof, which are treated as equivalent free-slip surfaces.

For the numerical computation, a 3-D single-precision separated solver and a k-ε RNG turbulence model are

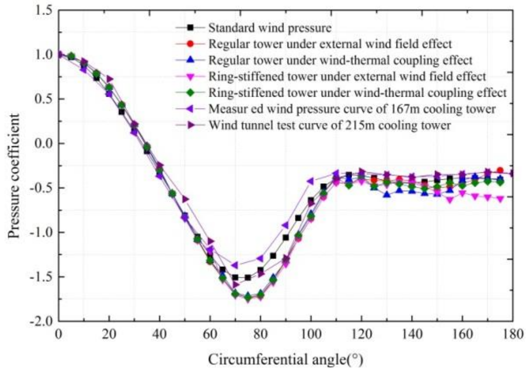

(a) external wind pressure coefficient

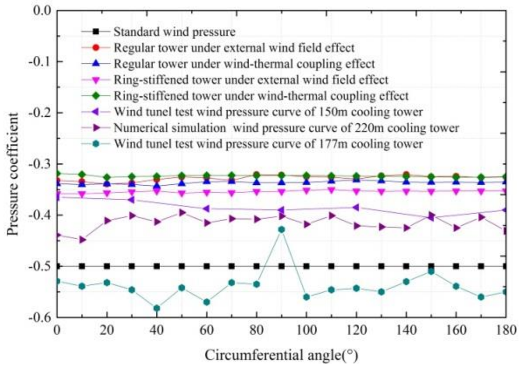

(b) internal wind pressure coefficient

Fig. 6 The numerically simulated average wind pressure compared with the standard and measured wind pressure

adopted, and the SIMPLE scheme is employed for solving the pressure-velocity coupling equations. For the gradient discretization, the Least Squares Cell based scheme is used for gradient discretization, the standard scheme is used for pressure discretization, the second-order windward scheme is used for power discretization, and the calculation residual of the scheme control equations is set to 10^{-6}.

3.3 Influences of natural convection and convective heat transfer

For large-scale indirect natural draft cooling systems, natural ventilation dry cooling is commonly adopted. The buoyancy force generated by natural convection drives the cooling air to circulate, thus the buoyancy force's influence must be considered during numerical simulation. When heat transfer takes place in a fluid, the fluid's density changes with its temperature, and the density variation plus gravity result in natural convection. The effect of buoyancy force on mixed convection can be measured by the ratio of the Grashof number to the Reynolds number.

$$\frac{Gr}{\mathrm{Re}^2}=\frac{\Delta\rho gh}{\rho v^2} \tag{3}$$

In the above equations, Gr is the Grashof number (the ratio of buoyancy to the viscous force), Re is the Reynolds number (the ratio of the inertia force to the viscous force), g is acceleration of gravity, ρ is density, ν is velocity, h is characteristic length. When the ratio is close to or exceeds 1.0, the influence of buoyancy force on convection is no longer negligible. For pure natural convection, the buoyancy induced flow is measured by the Rayleigh number.

$$Ra = g\beta\Delta TL^3\rho\big/\mu\alpha \tag{4}$$

$$\beta=-\frac{1}{\rho}\frac{\partial\rho}{\partial T} \tag{5}$$

$$\alpha=\frac{k}{\rho c_p} \tag{6}$$

In the above equations, Ra is the Rayleigh number, ΔT is temperature difference, β is the thermal expansion coefficient, α is the thermal diffusivity coefficient, k is coefficient of thermal conductivity and c_p is specific heat capacity. A Rayleigh number greater than 10^8 indicates that the convection driven by buoyancy force is a laminar flow. In order to correctly simulate natural convection, the energy equation is activated, include the effect of gravity, and the gas density is set to that of an incompressible gas. The radiators of the indirect natural draft cooling system are treated as equivalent heat sources inside the louvers. Convective heat transfer effect is considered for the calculation of fluid flow, and the heat boundary condition of the heat sources is defined as the convective heat transfer. The temperature of the heat sources is set to constant at 80℃ (353K), and the environmental temperature is set to 15℃ (288K).

3.4 Validation

To validate the effectiveness of the numerical simulation, the simulated average wind pressures are located in the cooling towers' outer and inner surface at throat height of 165 m and the standard and measured wind pressures are plotted in Fig. 6 for comparison. Fig. 7 presents the definition of circumferential angle, the range of θ is 0 ~ 360°. As can be seen, the curves of the average outer surface wind pressure are basically consistent with the standard curves (GB/T 50102-2014 2014; VGB-R 610Ue 2005) and measured wind pressure curves (Ke and Ge 2014, Cheng *et al.* 2014). The corresponding angles of the simulated extreme point and separation point of negative pressure and the windward values are all consistent with the standard and measured values, except that the negative pressure extremes are slightly less in magnitude than the standard and measured values. Evidently, the values obtained based on Reynolds means are valid. There are no consistent results in the existing results of internal wind pressure curves based on wind tunnel test or numerical

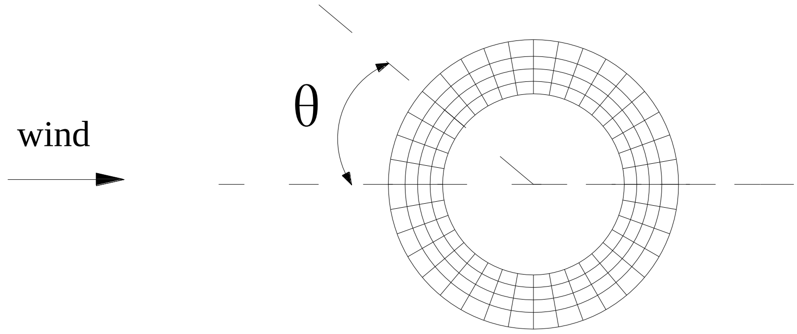

Fig. 7 The definition of circumferential angle

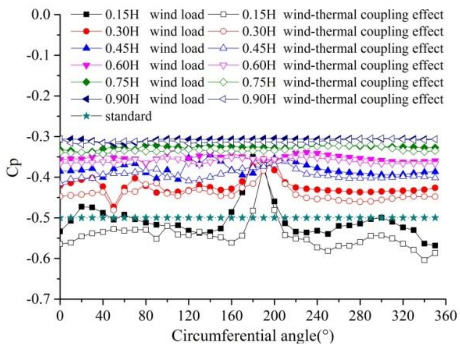

(a) Regular cooling tower

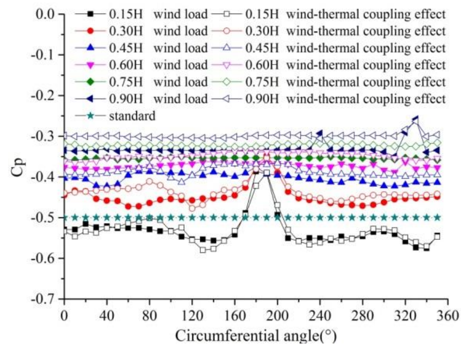

(b) Ring-stiffened cooling tower

Fig. 8 Comparisons of simulated internal pressure coefficients and standard value under different conditions

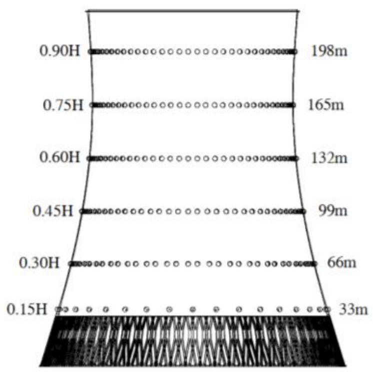

Fig. 9 The height of measuring points for cooling tower

simulation (Li *et al*. 2008, Shen *et al*. 2011, Zou *et al*. 2015). The internal pressure obtained by numerical simulation is slightly larger than parts of the results.

4. Analysis of internal pressure

4.1 Average wind pressure on the inner surface

Fig. 8 presents curves of the internal pressure coefficients of the cooling tower and the standard values (GB/T 50102-2014 2014; VGB-R 610Ue 2005) under different calculating conditions for comparison, and Fig. 9 shows the corresponding height of cooling tower. As can be seen, in the case where temperature field and internal stiffening ring beams are considered, the wind pressure on the inner surface is not uniformly distributed along the circumference nor the meridian direction. The absolute values of internal pressure coefficients gradually decrease with height and vary within the range of -0.6 to -0.3. At the lower bottom of the tower tube, the internal pressure coefficient is close to the standard value; the coefficient varies greatly along the circumference, especially at the leeward side, where the extremes of the coefficient occur. Around the tower throat (i.e., at 0.65 H, H is the total height of the tower), the internal pressure coefficient is basically

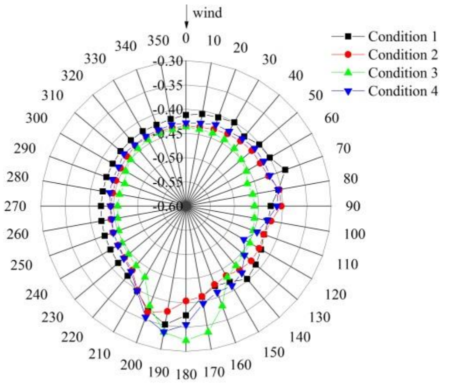

(a) Z = 72.944 m

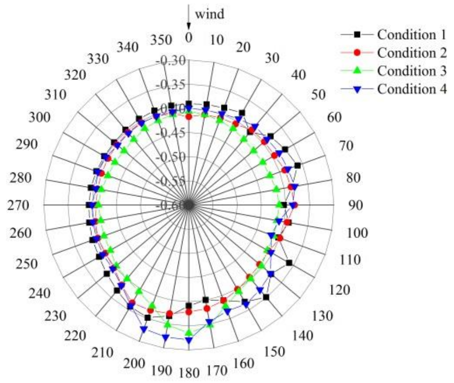

(b) Z = 94.955 m

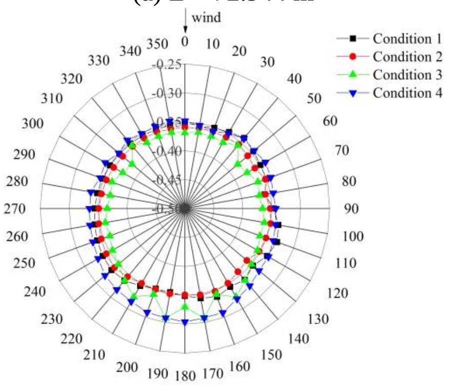

(c) Z = 139.628 m

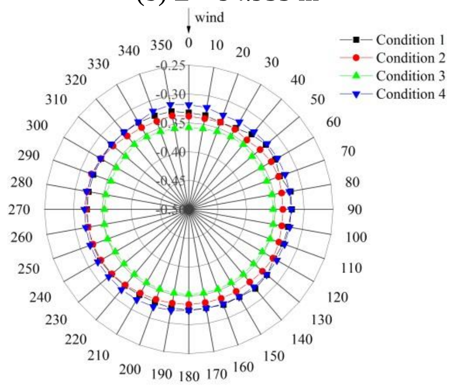

(d) Z = 165 m

Fig. 10 The internal pressure coefficients at typical cross-sections of the cooling tower under different conditions

evenly distributed along the circumference; however, the coefficient's value is to a certain extent different from the standard value, which is -0.50. When considering wind thermal coupling effect, the internal pressure coefficients of regular cooling tower are almost completely reduced, and as the height of tower increases, the degree of decrease gradually slows down. However, the internal pressure coefficients of ring-stiffened cooling tower have the opposite rule of those of the regular cooling tower. The maximum difference values of internal pressure coefficient are 0.057 of the regular cooling tower and 0.053 of the ring-stiffened cooling tower after temperature field is considered.

4.2 Influence of internal stiffening ring beams on internal pressure

Fig. 10 presents the circumferential distributions of internal pressure coefficient at the heights of the ring beams and the tower throat under different conditions, and Fig. 11 shows the height of three ring beams and throat. As can be seen, the ring beams change the flow field in the tower to a certain degree. At the heights where the ring beams are set, the internal pressure distributions under various conditions are different and show small fluctuations, especially at the leeward side. All the three ring beams are set below the tower throat, thus there is not direct obstruction of the beams at the throat. At the height of the tower throat, the internal pressure coefficient shows identical circumferential distribution patterns under different conditions and the distributions are basically uniform. When the temperature field is not considered, the existence of internal stiffening ring beams increases the absolute values of internal pressure coefficient; but decrements of the absolute values occur around the leeward side. With the temperature field considered, the existence of the ring beams decreases the absolute internal pressure coefficient.

In order to further analyze the uneven distributions of internal pressure coefficient in the cooling tower, the extreme values were calculated, as well as the differences between maximums and minimums, of the internal pressure coefficient at typical cross-sections under different conditions, as presented in Table 2.

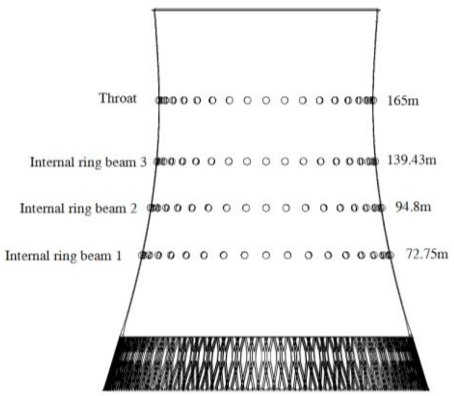

Fig. 11 The height of ring beams and throat for cooling tower

Table 2 Extremes of internal pressure coefficients at typical cross-sections of the cooling tower under different conditions

Height (m)	Parameter	Condition 1	Condition 2	Condition 3	Condition 4
72.944	$C_{pi,max}$	-0.352	-0.367	-0.323	-0.336
	$C_{pi,min}$	-0.429	-0.446	-0.465	-0.462
	ΔC_p	0.077	0.079	0.142	0.126
94.955	$C_{pi,max}$	-0.351	-0.366	-0.335	-0.321
	$C_{pi,min}$	-0.403	-0.417	-0.425	-0.419
	ΔC_p	0.052	0.051	0.090	0.098
139.628	$C_{pi,max}$	-0.331	-0.341	-0.308	-0.304
	$C_{pi,min}$	-0.360	-0.360	-0.381	-0.357
	ΔC_p	0.029	0.019	0.073	0.054
165	$C_{pi,max}$	-0.321	-0.321	-0.350	-0.316
	$C_{pi,min}$	-0.339	-0.343	-0.358	-0.326
	ΔC_p	0.019	0.022	0.008	0.011

As can be seen, the value ranges of the internal pressure coefficient under different conditions are different at different cross-sections. At the heights of the first, second, and third ring beams, and at the tower throat, the value ranges of the coefficient are -0.47~-0.32, -0.43~-0.32, -0.39~-0.30, and -0.36~-0.31, respectively. At the heights of the ring beams, the differences between maximums and minimums of the internal pressure coefficients are significantly larger than those in the cooling tower without stiffening rings. Meanwhile, at the tower throat, the difference is about half of that in the cooling tower without stiffening rings. Overall, in the regular tower without internal stiffening ring beams, the internal pressure coefficient is basically evenly distributed along the circumference with fluctuations smaller than 0.08. In the ring-stiffened tower, slight fluctuations occur at the leeward side of 120°~200°angles, where the internal pressure coefficient extremes have a difference of about 0.14.

4.3 Value of the internal pressure

Fig. 12 illustrates the vertical distributions of the internal pressure of the cooling tower under different conditions. As can be seen, the internal pressure coefficient is not evenly distributed vertically along the cooling tower, but shows a decreasing trend of the mean value as the height increases. When temperature field is not considered, the absolute internal pressure coefficient of the ring-stiffened tower is greater than that of the regular tower; however, when temperature field is considered, the existence of ring beams decreases the absolute internal pressure coefficient. For the regular tower, the negative pressure extreme is -0.51 when temperature field is not considered and -0.54 when it is considered; for the tower with stiffening rings, the former value increases by 5.12% and the latter value decreases by 2.37%. Under the four calculation conditions, the overall values of the internal pressure coefficient are -0.41, -0.43, -0.44, and -0.42, respectively. When the influences of temperature field and stiffening ring beams are considered, the internal pressure coefficient value is in the range of -0.45 to -0.40.

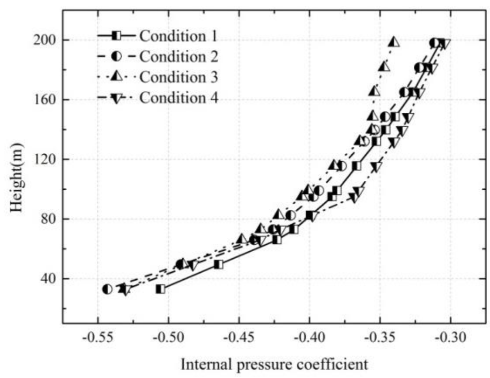

Fig. 12 The internal pressure coefficients the cooling tower under different conditions

The drag coefficients are defined as below.

$$C_{D,in} = \frac{\sum_{i=1}^{n} C_{pi,in} A_i \cos(\theta_i)}{A_T} \tag{7}$$

$$C_{D,\mathrm{ex}} = \frac{\sum_{i=1}^{n} C_{pi,\mathrm{ex}} A_i \cos(\theta_i)}{A_T} \tag{8}$$

$$C_D = C_{D,ex} - C_{D,in} \tag{9}$$

In the above equations, C_D is local drag coefficient, $C_{D,in}$ is internal drag coefficient, $C_{D,ex}$ is external drag coefficient, $C_{pi,in}$ is internal pressure coefficient of measuring point i, $C_{pi,ex}$ is external pressure coefficient of measuring point i, A_i is covered area of measuring point i, A_T is the area of structure along-wind, θ is angle between the measuring point and wind. Table 3 presents the value of local drag

Table 3 Drag coefficients at typical cross-sections of the cooling tower under different conditions

Height (m)	Parameter	Condition 1	Condition 2	Condition 3	Condition 4
33	$C_{D,ex}$	0.330	0.272	0.380	0.297
	$C_{D,in}$	-0.031	-0.034	-0.025	-0.023
	C_D	0.361	0.306	0.406	0.320
66	$C_{D,ex}$	0.366	0.348	0.452	0.381
	$C_{D,in}$	-0.014	-0.022	-0.024	-0.015
	C_D	0.380	0.371	0.476	0.396
72.944	$C_{D,ex}$	0.381	0.334	0.488	0.411
	$C_{D,in}$	-0.011	-0.019	-0.042	-0.023
	C_D	0.392	0.352	0.530	0.435
94.995	$C_{D,ex}$	0.429	0.376	0.510	0.502
	$C_{D,in}$	-0.014	-0.017	-0.033	-0.034
	C_D	0.443	0.393	0.543	0.536
99	$C_{D,ex}$	0.431	0.409	0.512	0.500
	$C_{D,in}$	-0.013	-0.016	-0.033	-0.034
	C_D	0.445	0.425	0.545	0.534
132	$C_{D,ex}$	0.357	0.333	0.318	0.390
	$C_{D,in}$	-0.009	-0.010	-0.033	-0.031
	C_D	0.366	0.343	0.351	0.421
139.628	$C_{D,ex}$	0.279	0.289	0.238	0.282
	$C_{D,in}$	-0.008	-0.009	-0.033	-0.030
	C_D	0.287	0.298	0.271	0.312
165	$C_{D,ex}$	0.053	0.116	0.133	0.078
	$C_{D,in}$	-0.004	-0.003	-0.003	0.000
	C_D	0.057	0.119	0.136	0.078
198	$C_{D,ex}$	0.078	0.106	0.013	0.050
	$C_{D,in}$	-0.003	0.003	-0.010	0.045
	C_D	0.080	0.103	0.023	0.006

coefficient, the internal drag coefficient and the external coefficient at typical cross-sections under different conditions. As can be seen, the internal drag coefficient is smaller than the drag coefficient on the outer surface; vertically, the internal drag coefficient value varies in the range of -0.05 to 0.05. The influence of stiffening rings on the internal drag coefficient is similar to that on the internal pressure coefficient. However, when temperature field is considered, the internal drag coefficient has higher absolute values within the height range of the ring beams compared to those in the regular tower. The value of the local drag coefficients of the regular tower have higher values compared to those in ring-stiffened cooling tower, meanwhile the value of the local drag coefficients decrease when wind-thermal coupling considered.

5. Analysis of flow mechanism

5.1 Internal and external flow fields

Fig. 13 presents the velocity vector diagrams of the flow fields inside and outside the regular tower under the effect of an external wind field. As can be seen, the incoming flow diverts at the windward side of the tower, detours around the two sides of the tower and forms vortexes of various sizes at the leeward side. Part of the incoming flow enters the tower via the opening of the louvers and the air flows and collides with the curved surface inside the tower and moves towards the tower top; the necking effect of the tower throat results in a large vortex area near the throat. At the tower top, an apparent three-dimensional effect appears; the incoming flow sweeps over the top and meets the upward flow from the tower, accelerating the air flow inside the tower near the top, and creating large-scale vortex shedding at the tower top leeward area. The collision between the incoming flow entered the tower from the louver and the tower tube’s inner surface on the leeward side, together with the three-dimensional detouring flow near the ground, create large-scale vortexes at the leeward side near the ground.

To investigate the difference of the internal flow resultant from the addition of stiffening ring beams, the velocity streamlines of the internal and external flow fields

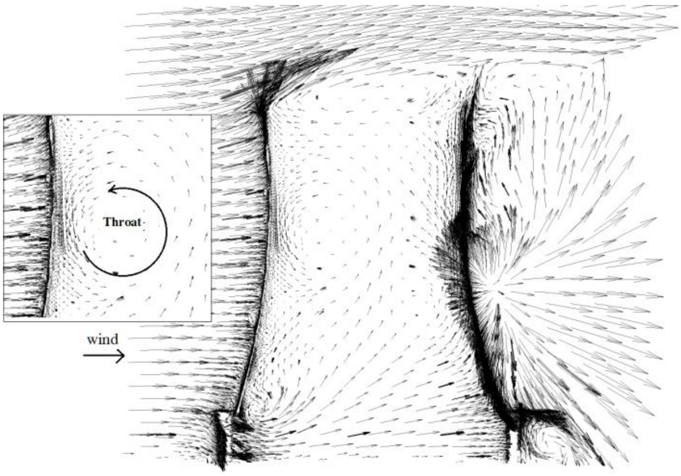

Fig. 13 Velocity vector of flow fields of the cooling tower under external wind load

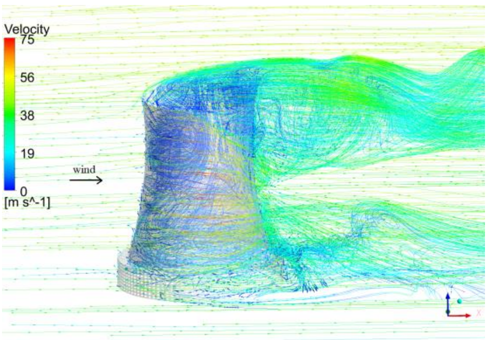

(a) Condition 1

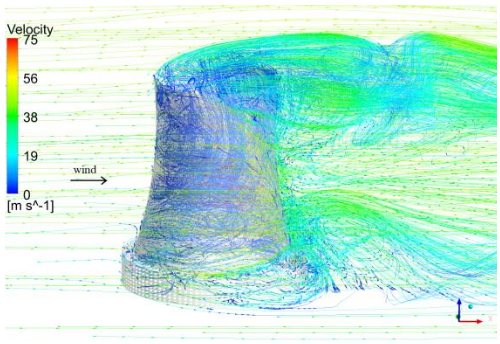

(b) Condition 2

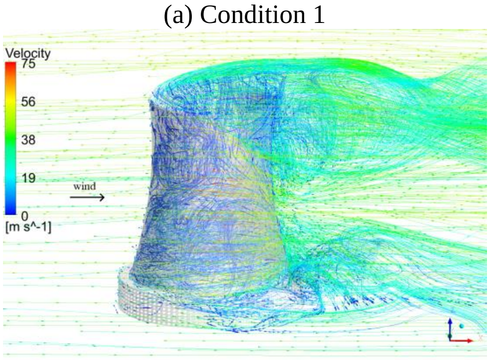

(c) Condition 3

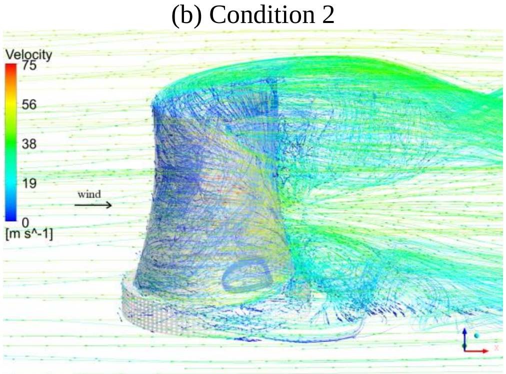

(d) Condition 4

Fig. 14 Velocity streamlines of the internal and external flow fields of the cooling tower under different conditions

of the cooling tower under different conditions are plotted, as shown in Fig. 14. Fig. 15 presents velocity streamlines of x-z plane of the cooling tower under different conditions. As can be seen, the incoming flow inside the tower collides with the leeward inner surface and rises up to the tower top; the upward air flow near the windward side is affected by the external incoming flow and changes its direction, thus forming a inverse flow; at this time, the vortex is mainly formed at the tower throat near the windward side. The ring-stiffened tower, however, has three ring beams below the throat; when the air flow rises along the leeward inner surface of the tower, its direction changes when it meets each stiffening ring beam, causing the air flow inside the tower to be disordered. The specific performance is the difference of the scale and position of the vortex in the tower. When the temperature field is considered, due to the existence of the heat sources inside the louvers, the air flow in the tower is more complicated compared to that when temperature field is not considered. In the ring-stiffened tower, the air flow forms a triangular loop at the tower bottom; meanwhile, vortexes continuously shed, move upwards along the windward side, and mix with the flow at

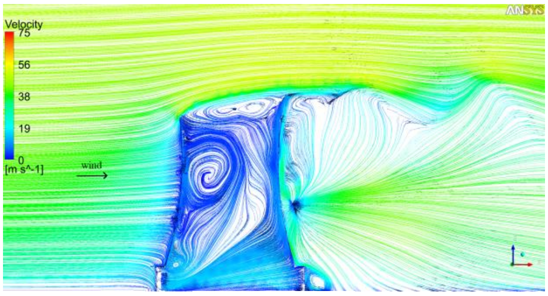

(a) Condition 1

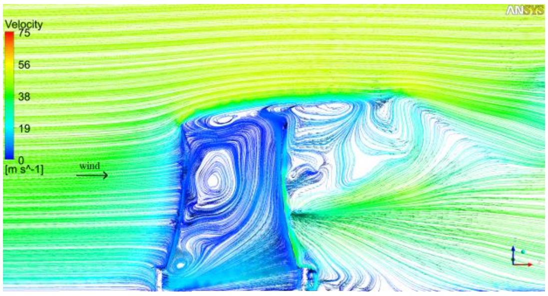

(b) Condition 2

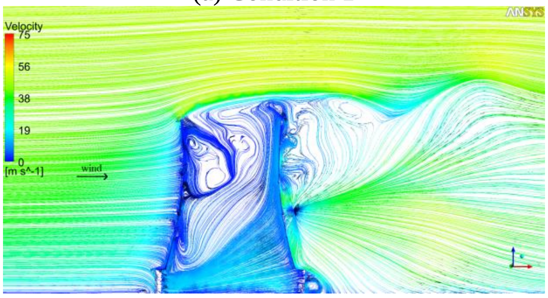

(c) Condition 3

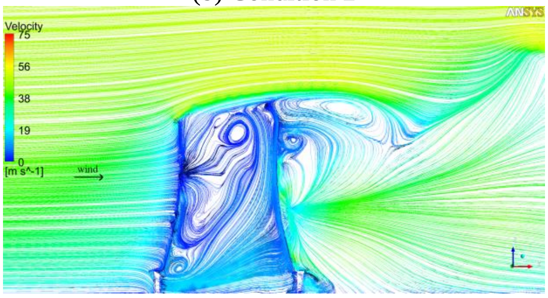

(d) Condition 4

Fig. 15 Velocity streamlines of x-z plane of the cooling tower under different conditions

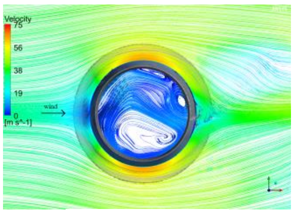

(a) Condition 1

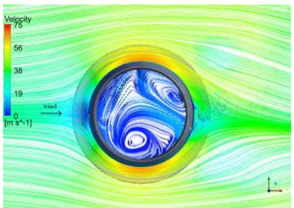

(b) Condition 2

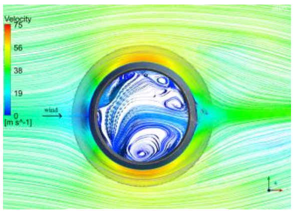

(c) Condition 3

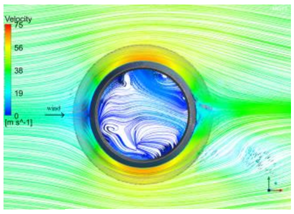

(d) Condition 4

Fig. 16 Velocity Streamlines at the height of the first ring beam on the x-y cross-section

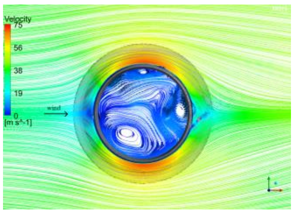

(a) Condition 1

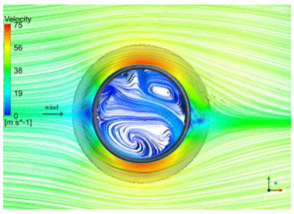

(b) Condition 2

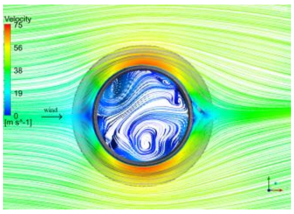

(c) Condition 3

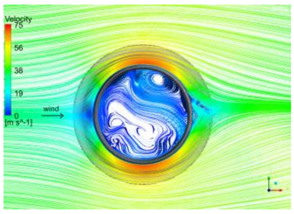

(d) Condition 4

Fig. 17 Velocity Streamlines at the height of the second ring beam on the x-y cross-section

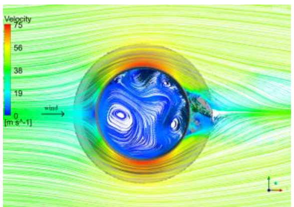

(a) Condition 1

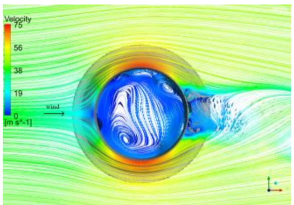

(b) Condition 2

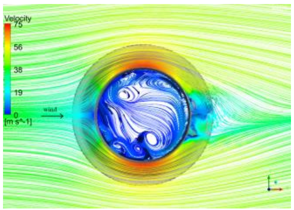

(c) Condition 3

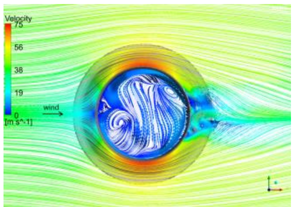

(d) Condition 4

Fig. 18 Velocity Streamlines at height of third ring beam on the x-y cross-section

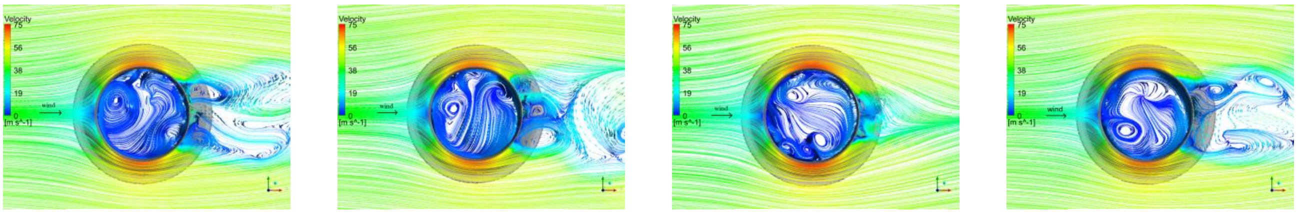
(a) Condition 1 (b) Condition 2 (c) Condition 3 (d) Condition 4

Fig. 19 Velocity Streamlines at the height of the tower throat on the x-y cross-section

the windward side, making the air flow inside the tower more chaotic.

Inside the cooling tower, the incoming flow collides with the leeward inner surface of the tower and rotates along the inner surface and rises up. With the stiffening ring beams inside the tower, the air flow changes significantly. In order to further analyze the influence of the ring beams on the pressure distribution inside the tower, the velocity streamlines at the heights of the three beams and at the tower throat under different conditions are plotted, as shown in Figs. 16-19.

From the plotted velocity streamlines, the followings can be observed. 1) The incoming flow diverts at the windward side of the cooling tower, detours around the outer surface and accelerates as it passes the two sides of the tower, and form vortexes of various sizes at the leeward side; vortex shedding occurs afterward. Due to the necking effect of the cooling tower at the throat area and that all three ring beams are below the throat, the acceleration of the flow in the velocity gain zones at the two sides of the tower becomes more obvious as the height increases. 2) At the height of the first ring beam, the air flow inside the tower is not changed significantly by the ring beam. Vortexes form at the sides and the leeward area, and the interaction between them changes the location of the flow on the leeward inner surface. Under conditions 1, 2, and 4, the vortexes make the flow direction inclined; the flow collides with the inner surface at the angle of 190° ~ 200°, which corresponds to the negative pressure extremes under these conditions. Under condition 3, the incoming flow angle changes to 180°, which also corresponds to the negative pressure extreme. 3) At the height of the second ring beam, the flow changes more significantly than that at the first ring beam. If the temperature field is considered, the vortex size increases. If the temperature field is not considered, the cross-sectional flow of the regular tower forms three major vortexes. In the ring-stiffened tower, the vortex near the windward side moves backwards and drives surrounding air flow to form larger vortexes. With the temperature field considered, two vortexes form, and the extremes of the inner surface negative pressure occur at the angle of 180° on the leeward side. 4) At the height of the third ring beam, the internal flow of the tower changes significantly, whereas the flow at the leeward side outside the tower changes significantly as well. If the temperature field is not considered, the internal flow is obstructed by the ring beam to a certain extent and forms multiple vortexes. If the temperature is considered, the vortexes move towards the windward side; at the leeward side, the internal flow moves along the tower shell in an adhesive manner, thus there is not significantly increased negative pressure extreme at the leeward side at this height. 5) At the tower throat, the internal flow moves along the tower shell. Since the three ring beams have changed the upward internal flow, the flow in the ring-stiffened tower at the throat is greatly different from that in the regular tower. The vortex concentrated area moves towards the two sides from the windward side, and the vortexes become smaller. Due to the wind-thermal coupling effect, vortex shedding is more serious at the leeward side of the ring-stiffened tower.

5.2 Characteristics of the temperature field

Figs. 20 and 21 present the temperature distributions at typical cross-sections of the conventional tower and the ring-stiffened tower with temperature field considered. As can be seen, the existence of the three ring beams significantly changes the distribution of the temperature field; from the tower bottom to the tower top, the temperature gradually decreases and degree of decrement differs significantly from that in the conventional tower. Part of the incoming flow in the external wind field enters the tower via the louvers, drives the hot air flow inside the tower to move and the heat gradually dissipates as the flow rises upwards. Inside the louvers of the windward side, the temperature is relatively low, and a temperature gain zone forms at the wind inlet; near the leeward side inside the tower, the temperature is relatively high. The three inner ring beams are set in the middle and lower part of the tower, and a certain disturbance and obstruction are performed to the rising air flow in the tower. The ring-stiffened tower shows the temperature reduction in the throat to the top, and the temperature gain zones mainly occur below the throat. Meanwhile, it can be seen that because of the ring beams, the temperature decreases in large-scale areas at the leeward side of the tower top. As the temperature distributions at the wind inlets and outlets show, the temperature increasing area at the inlet occurs at the side back of the tower for the conventional tower; for the ring-stiffened tower, the areas of higher temperature mainly occur at the windward side, and the temperature distribution is relatively uniform at the outlet. For the conventional tower, the mean temperature is 305.6 K for the inlet cross-section and 304.9 K for the outlet cross-section. For the ring-stiffened tower, the mean temperature is 307.6 K for the inlet cross-section and 305.3 K for the outlet cross-section. The pressure increases with the increase of temperature in the ring-stiffened tower, and the absolute value of the internal pressure inside the tower

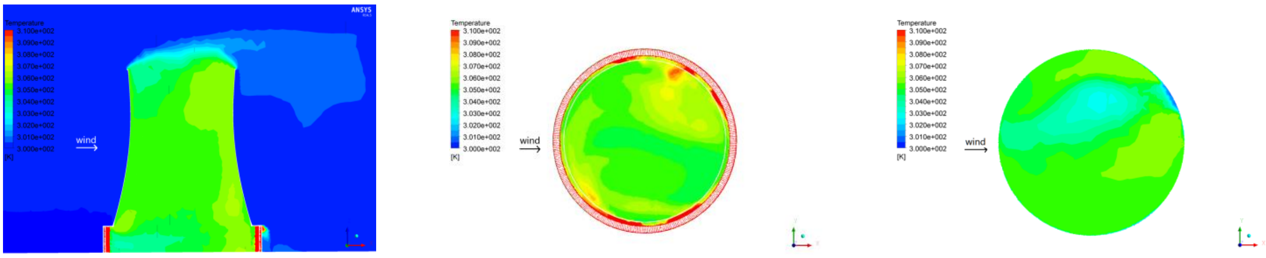

(a) x-z cross-section (b) inlet cross-section (c) outlet cross-section

Fig. 20 Temperature distributions of the conventional cooling tower under wind-thermal coupling effect

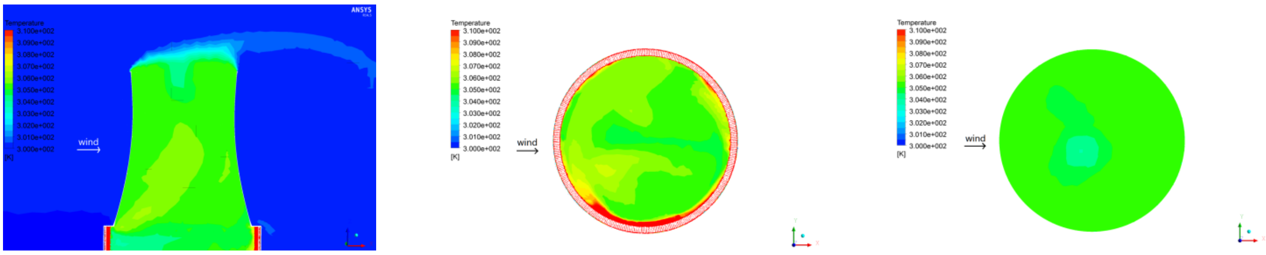

(a) x-z cross-section (b) inlet cross-section (c) outlet cross-section

Fig. 21 Temperature distributions of the cooling tower with rings under wind-thermal coupling effect

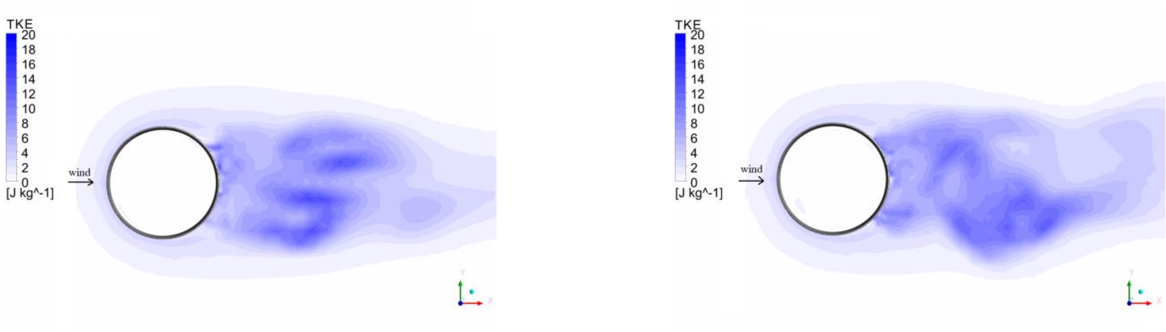

(a) Condition 1 (b) Condition 2

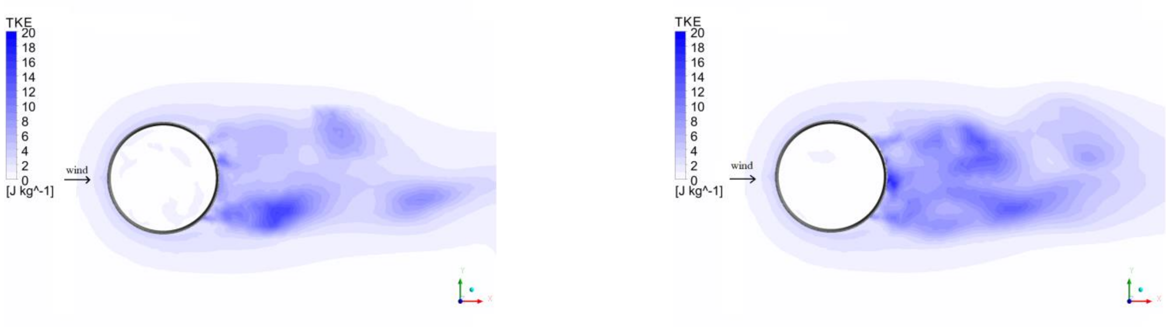

(c) Condition 3 (d) Condition 4

Fig. 22 TKE distributions at the throat cross-section of the cooling tower under different conditions

decreases with the superposition of the pressure under the wind load. Indicating that the existence of the three ring beams to a certain extent hinders the flow and heat dissipation.

5.3 The turbulence kinetic energy

Turbulence kinetic energy (TKE) measures the intensity of turbulence. Figs. 22 and 23 present the TKE distributions at the tower throat and x-z cross-sections of the cooling tower under different conditions. As can be seen, the

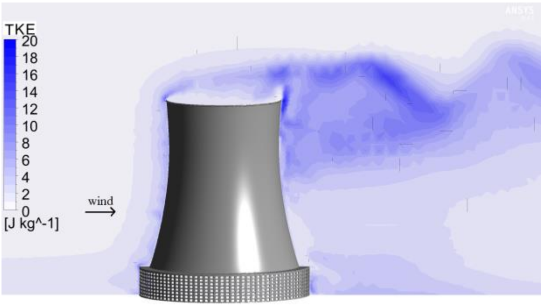

(a) Condition 1

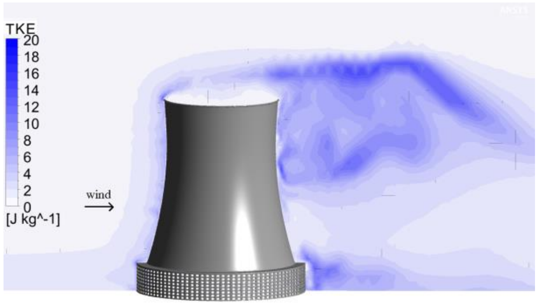

(b) Condition 2

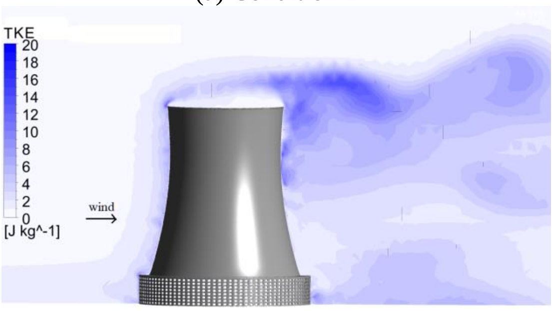

(c) Condition 3

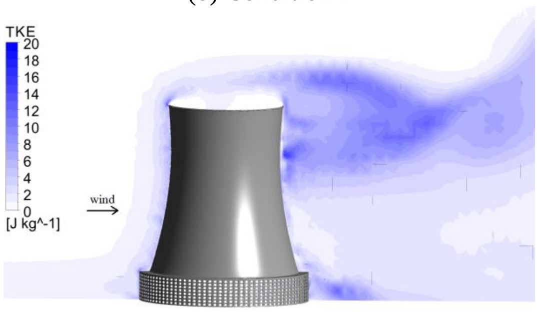

(d) Condition 4

Fig. 23 TKE distributions at the x-z cross-section of the cooling tower under different conditions

existence of the ring beams alters the flows inside and outside the cooling tower. The changes of the flow vortexes' locations and sizes result in differences in the TKE distributions of the cooling towers; the TKEs at the leeward side of the ring-stiffened tower are lower than those of the conventional tower. With the effect of the temperature field considered, an obvious TKE gain area appears at the throat cross-section; the area corresponds to the vortex formation area, indicating that the formation of large-size vortexes causes the turbulence intensity to increase. Under the four calculation conditions, the average values of the TKE at the throat cross-section are 0.468 $J \cdot kg^{-1}$, 0.415 $J \cdot kg^{-1}$, 0.595 $J \cdot kg^{-1}$, and 0.4 $J \cdot kg^{-1}$, respectively. When temperature field is considered, the average TKE of the throat section of the regular tower and the ring-stiffened tower were reduced. In particular, the average TKE of the ring-stiffened tower decreased by 32%. When temperature field is not considered, the average TKE of the ring-stiffened tower is greater than that of the regular tower; however, when temperature field is considered, the existence of ring beams decreases the average TKE. As the x-z cross-sectional TKE distributions show, the primary leeward TKE gain area appears at the louvers and the wind inlet. Under the wind-thermal coupling effect, the area's TKE is significantly higher than that under solely external wind field effect, indicating that the flow field around the cooling tower is more complicated when wind-thermal coupling effect is considered.

5.4 Influence of the wind resistance

Fig. 24 presents the pressure distributions at the x-y cross-section of the cooling tower under different conditions. Based on the distributions, the followings can be seen. 1) When the temperature field is not considered, the existence of the internal stiffening ring beams increases the absolute internal negative pressure. When the temperature field is considered, the existence of the ring beams increases the absolute internal negative pressures at the lower bottom and the leeward air outlet of the cooling tower and decreases the absolute negative pressure near the tower top. 2) Under the wind-thermal coupling effect, the absolute pressure inside the conventional tower is significantly higher than that under the effect of the external wind-field, indicating that the consideration of the temperature field decreases the internal negative pressure, i.e. increases the absolute value. 3) With the temperature field considered, the absolute pressure above the throat of the ring-stiffened tower decreases. 4) At the leeward tower top area, the absolute pressure under the wind-thermal coupling effect is significantly lower than that under the effect of the external wind field.

To study the influence of the temperature field on the air flow lifting inside the tower, the pressures at the wind inlet and outlet are compared. Figs. 25 and 26 present the pressure distributions at the inlet and outlet cross-sections of the cooling tower under different conditions. Under condition 1, the mean pressures at the inlet and outlet are -415.9 Pa and -418.6 Pa, respectively, with a pressure difference of 2.7 Pa. Under condition 2, the mean pressures at the inlet and outlet are -416.1 Pa and -445.1 Pa, respectively, with a pressure difference of 29.0 Pa. Under condition 3, the mean pressures at the inlet and outlet are -436.4 Pa and -449.4 Pa, respectively, with a pressure difference of 13 Pa. Under condition 4, the mean pressures at the inlet and outlet are -435.5 Pa and -400.6 Pa, respectively, with a pressure difference of 33.9 Pa. In both cases, under external wind field effect and under wind-

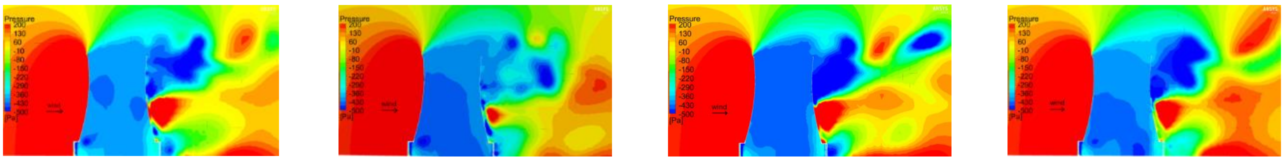

(a) Condition 1 (b) Condition 2 (c) Condition 3 (d) Condition 4

Fig. 24 Pressure distributions at the x-y cross-section of the cooling tower under different conditions

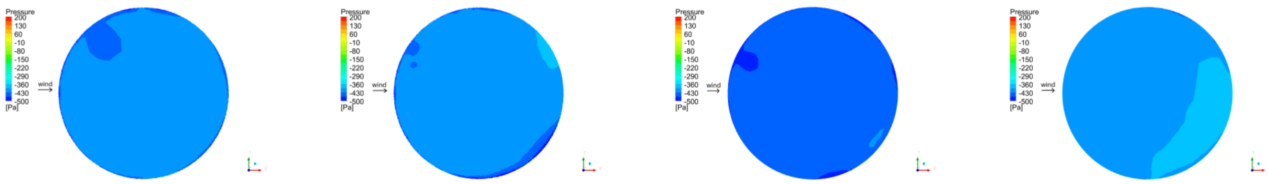

(a) Condition 1 (b) Condition 2 (c) Condition 3 (d) Condition 4

Fig. 25 Pressure distributions at the inlet cross-section of the cooling tower under different conditions

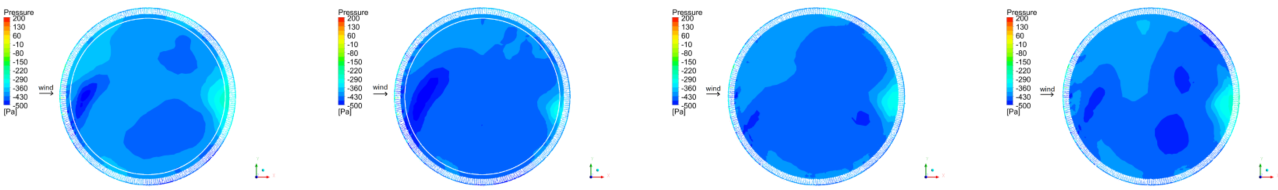

(a) Condition 1 (b) Condition 2 (c) Condition 3 (d) Condition 4

Fig. 26 Pressure distributions at the outlet cross-section of the cooling tower under different conditions

thermal coupling effect, the existence of ring beams increases the pressure difference between the inlet and outlet, and the difference in the former case is more significant.

6. Conclusions

- In this study, equivalent heat source and coupled numerical algorithm are adopted to study the internal pressure distribution and flow field mechanism of cooling towers under wind-thermal coupling effect. The result is in good accordance with existing studies. It is validated that the approach is effective for the numerical simulation of the internal flow field in an operating cooling tower with the influences of peripheral radiators considered.
- With the influences of radiators considered, the inner surface of the cooling tower is under the effects of both wind load and temperature. Adding stiffening ring beams significantly changes the pressure and temperature field distributions, increases the pressure difference between the wind inlet and outlet, and decreases the temperature inside the tower. In addition, the temperature is higher at both the inlet and the outlet compared to the conventional tower. The existence of the ring beams, to a certain extent, hinders the flow and heat dissipation, generating adverse influences on the internal flow of the cooling tower.
- The incoming flow diverts at the windward side of the tower shell, detours around the tower, and forms vortexes of various sizes at the leeward side of the tower. An apparent three-dimensional effect appears at the tower top; the incoming flow sweeps over the top and meets the upward flow from the tower, accelerating the air flow inside the tower near the top. Part of the incoming flow enters the tower shell via the opening of the louvers and the air flows and collides with the curved inner surface of the tower and moves towards the tower top. The air flow close to the inner surface is obstructed by the ring beams and changes its direction; the air flow collides with the tower shell disorderly, making the flow more chaotic compared to that in the conventional tower without stiffening ring beams.
- Analysis of the internal pressure distributions under different conditions shows that the wind pressure on the inner surface of the cooling tower is not uniformly distributed along the meridian and circumferential directions. At the lower bottom of the tower, the internal pressure coefficient varies significantly along the circumference, and as the height increases, the circumferential distribution of the coefficient gradually becomes uniform. In particular, at the heights of the ring beams, the internal pressure coefficient varies greatly at the angle of 120° ~ 200° at the leeward side, and the maximum difference between the extremes of the coefficient is about 0.14. With the influences of temperature field and internal ring beams considered,

the internal pressure coefficient of the cooling tower is in the value range of -0.45 to -0.40.

- The heat from peripheral radiators of the cooling tower has significant influence on the internal pressure. When the temperature field is not considered, the absolute internal pressure coefficient of the ring-stiffened tower is greater than that of the conventional tower; the ring beams increase the coefficient's absolute value by 7.32%. With the temperature field considered, the absolute internal pressure coefficient of the ring-stiffened tower decreases by 2.33%. Overall, the coefficient value of -0.42 for ring-stiffened cooling tower under wind-thermal coupling effect is suggest.

Acknowledgments

This project is jointly supported by National Natural Science Foundation (51878351, 51761165022, U1733129, 51208254), Jiangsu Province Outstanding Natural Science Foundation (BK20160083), Jiangsu Qinglan Project and Postdoctoral Science Foundation (2013M530255, 1202006B), which are gratefully acknowledged.

References

Babu, G.R. Rajan, S.S., Harikrishna, P. *et al.* (2013), "Experimental Determination of Wind-Induced Response on a Model of Natural Draught Cooling Tower", *Exp. Techniques*, **37**(1), 35-46.

Burger, A.A.S. (2014), "Numerical analysis of flow around infinite and finite cylinders at trans-critical Reynolds numbers with and without surface roughness", *University of Sussex*, **40**(4), 219-242.

Cheng, X.X., Zhao, L., Ge, Y.J. *et al.* (2015), "Wind pressures on a large cooling tower", *Adv. Struct. Eng.*, **18**(2), 201-220.

Dong, G.C., Zhang, J.R., Cai, C.S. *et al*. (2015), "Numerical simulation of internal surface pressure coefficient of super-large cooling tower under operating conditions", *J. Hunan Univerisity (Naturnal Science)*, **42**(1), 17-23. (In Chinese)

Dong, G.C., Zhang, J.R., Cai, C.S. *et al.* (2016), "Study of internal surface pressure coefficient of super-large cooling tower with different internal main components", *Eng. Mech.*, **33**(4), 77-83. (In Chinese)

Du, X.P., Yin, Y., Zeng, M. *et al.* (2014), "An experimental investigation on air-side performances of finned tube heat exchangers for indirect air-cooling tower", *Therm. Science*, **18**(3), 863-874.

GB 50009-2012 (2012), *Load code for the design of building structures*, The Ministry of Construction of China, Beijing, China, 35-36. (In Chinese)

GB/T 50102-2014 (2014), *Code for design of cooling for industrial recirculating water*, The Ministry of Construction of China, Beijing, China, 24-25 (In Chinese)

Goudarzi, M.A. and Sabbagh-Yazdi, S.R. (2011), "Effects of modeling strategy on computational wind pressure distribution around the cooling tower's", *Wind Struct.*, **14**(1), 81-84.

Gu, H., Wang, H., Gu, Y. *et al.* (2016), "A numerical study on the mechanism and optimization of wind-break structures for indirect air-cooling towers", *Energ. Convers. Manage.*, **108**, 43-49.

JGJ/T 338-2014 (2014), Standard for wind tunnel test of buildings and structures, The Ministry of Construction of China, Beijing, China, 16-17. (In Chinese)

Kasperski, M. and Niemann, H.J. (1988), "On the correlation of dynamic wind loads and structural response of natural-draught cooling towers", *J. Wind Eng. Ind. Aerod.*, **30**(1-3), 67-75.

Kawarabata, Y., Nakae, S. and Harada, M. (1983), "Some aspects of the wind design of cooling towers", *J. Wind Eng. Ind. Aerod.*, **14**, 167-180.

Ke, S.T., Ge, Y.J. and Zhao, L. (2015), "Wind-induced vibration characteristics and parametric analysis of large hyperbolic cooling towers with different feature sizes", *Struct. Eng. Mech.*, **54**(5), 891-908.

Ke, S.T., Liang, J., Zhao, L. *et al*. (2015), "Influence of ventilation rate on the aerodynamic interference between two extra-large indirect dry cooling towers by CFD", *Wind Struct.*, **20**(3), 449-468.

Ke, S.T., Yu, W., Zhu, P. *et al*. (2018), "Full-scale measurements and damping ratio properties of cooling towers with typical heights and configurations", *Thin-Wall. Struct.*, **124**, 437-448.

Li, P.F., Zhao, L., Ge, Y.J. *et al.* (2014), "Wind tunnel investigation on wind load characteristics for super large cooling towers", *Eng. Mech.*, **25**(6), 60-67. (In Chinese)

Li, X., Gurgenci, H., Guan, Z. *et al.* (2017), "Measurements of crosswind influence on a natural draft dry cooling tower for a solar thermal power plant" , *Appl. Energ.*, **206**, 1169-1183.

Sabouri-Ghomi, S., Kharrazi, M.H.K. and Javidan, P. (2006), "Effect of stiffening rings on buckling stability of R.C. hyperbolic cooling towers", *Thin-Wall. Struct.*, **44**(2), 152-158.

Shen, G.H., Yu, G.P., Sun, B.N. *et al*. (2011), "Analysis of wind load on large hyperbolic cooling tower considering interaction between internal and external pressure", *Acta Areodynam. Sinica*, **29**(4), 439-446. (In Chinese)

Shen, G.H., Zhang, C.S., Sun, B.N. *et al.* (2011), "Numerical simulation of wind load on inner surface of large hyperbolic cooling tower", *J. Harbin Institute of Technology*, **43**(4), 104-108. (In Chinese)

Sollenbercer, N.J. and Billington, D.P. (1980), "Wind loading and response of cooling tower", *J. Struct. Div. - ASCE*, **106**(3), 601-621.

Sun, T.F. and Zhou, L.M. (1983), "Wind pressure distribution around a ribless hyperbolic cooling tower", *J. Wind Eng. Ind. Aerod.*, **14**(1), 181-192.

VGB-R610Ue (2005), VGB-Guideline: Structural design of cooling tower-technical guideline for the structural design, computation and execution of cooling tower, Essen: BTR Bautechnik Bei Kühltürmen.

Widodo, T. and Riyadi, B. (2014), "A parametric study of wind catcher model in a typical system of evaporative cooling tower using CFD", *Appl. Mech. Mater.*, **660**, 659-663.

Wittek, U. and Grote, K. (2015), "Substitute wind concept for elastic stability of cooling tower shells", *Mater. Member Behavior*, 500-513.

Zhang, J.F., Chen, H., Ge, Y.J. *et al.* (2014), "Effects of stiffening rings on the dynamic properties of hyperboloidal cooling towers", *Struct. Eng. Mech.*, **49**(5), 619-629.

Zhao, L. and Ge, Y.J. (2010), "Wind loading characteristics of super-large cooling towers", *Wind Struct.*, **13**(3), 257-273.

Zhao, L., Chen, X., Ke, S.T. and Ge, Y.J. (2014), "Aerodynamic and aero-elastic performances of super-large cooling towers", *Wind Struct.*, **19**(4), 443-465.

Zou, Y.F., He, X.H., Chen, Z.Q. *et al*. (2015), "Wind tunnel test and numerical simulation study on internal wind loading for super large cooling tower", *Acta Areodynam. Sinica*, **33**(5), 697-705. (In Chinese)

Zou, Y.F., He, X.H., Tan, L.X. *et al.* (2015), "Three-dimensional effect and design value of inter surface wind loading for single super-large cooling tower", *J. Hunan University (Natural Sciences)*, **42**(1), 24-30. (In Chinese)

CC